Proceedings of the Canadian Society for Mechanical Engineering International Congress 2021
CSME Congress 2021
June 27-30, 2021, Charlottetown, PE, Canada

INVESTIGATION INTO THE ONSET OF TURBULENT RAYLEIGH-BENARD CONVECTION USING TIME-RESOLVED 2-D PARTICLE IMAGE VELOCIMETRY

Sina Kashanj and David S. Nobes*
Mechanical Engineering Department, University of Alberta, Edmonton, Canada
*dnobes@ualberta.ca

Abstract— The flow topology for the onset of the convection has been studied experimentally applying time-resolved 2-D PIV (Particle Image Velocimetry) to the turbulent RBC (Rayleigh-Benard Convection) in a cubical enclosure with unit aspect ratio for Rayleigh number of 5.5×10^7 and Prandtl number of 6.98. Experiments have been undertaken over a time duration of 2800 s. The results of the mean convection are presented and compared with the instantaneous flow structures at the final state of the flow from 2450 s to 2800 s. Then, the flow topology at the onset of the convection is presented. A mean flow pattern is found for the onset of convection that contains two large scale circulating patterns.

Keywords: Rayleigh-Benard convection; Buoyancy driven flow; Large scale circulation;Convective turbulent flow; Particle Image Velocimetry (PIV)

I. INTRODUCTION

Buoyancy-driven flow in an enclosure heated from below and cooled from above is known as Rayleigh-Benard Convection (RBC) [1]. RBC is an idealized flow system to study the flow and heat transfer of a wide spectrum of phenomena and applications [2]. In engineering, RBC can be studied to investigate the natural convective turbulent flow in closed systems [2]. To understand the physics of the complex convective flows that occur in nature, such as the flow inside planets and their atmospheric flows, this simple system has been a focus of investigation [3, 4].

For low and moderate Rayleigh numbers, it is shown that the steady-state roll structures form in RBC cell [5]. Pallares et al. [6] investigated the flow structures of a cubical RBC with the Rayleigh number changing in the range of $5\times10^3 < Ra < 8\times10^4$ applying PIV. For this range of Rayleigh number they reported formation of a steady-state single roll structure [6].

For high Rayleigh numbers, it is shown that the number of turbulent roll structures is time-dependent [13]. It is noteworthy that the heat transfer of the heat source and sink surfaces is dependent on the number of these turbulent structure rolls which is lower for the higher number of them [7]. This dependency is different for different scenarios. For example, for RBC enclosures with an aspect ratio lower than one (i.e. equal size of width and side both lower than the height of the enclosure), by decreasing the aspect ratio, the frequency of fluctuations in the number of the turbulent roll structures increases [8]–[13].

Although the size and numbers of the turbulent roll structures are time-dependent, the mean flow leads to a large-scale mean flow showing the single roll structure dominancy [14]. This large scale mean flow is known as large scale circulation (LSC) which sometimes is referred as the mean wind in RBC studies [14].

Both in laminar and turbulent RBC, it has been accepted that the formation of LSCs is due to the momentum of the thermal plumes added to the global flow from the heat and sink surfaces [15]–[17]. The final state of the thermal plumes temporal journey is known as the mean wind [16]. It is known that reaching the final state of the flow in turbulent RBC starts with the rising and falling of the hot and cold plumes [5]. Yet, the flow topology of the onset of the convection is missed due to the attention of studies to the final state of the turbulent RBC. Xi et al. [5] showed that the time scale of the onset of the turbulent RBC could be in the same order of the considered final state, $t_{onset} \sim 0.8\ t_{mean\ wind}$ which shows the importance of the onset of convection.

In this paper, the flow topology of the onset of the convection has been studied experimentally applying time-resolved 2-D PIV in the turbulent RBC in a cubical enclosure with unit aspect ratio, $Ra = 5.5 \times 10^7$, and $Pr = 6.98$. The aim of this investigation is to identify a possible mean flow at the onset of the convection in a time scale similar to the mean wind.

II. PHYSICS OF RBC

The regime of RBC is characterized by the Rayleigh number, Ra represents the ratio of the time scale for the thermal transport by diffusion to the time scale of the thermal transport by convection [1] and is defined as:

$$Ra = \frac{\alpha g H^3 (T_H - T_C)}{\nu \kappa} \quad (1)$$

Here, α is the thermal expansion coefficient, g is gravitational acceleration, ν is kinematic viscosity, and κ is thermal

diffusivity of the fluid. In this equation, T_H and T_C represent the temperature of the hot and cold surfaces respectively. The Rayleigh number also depends on the height, H of the RBC cell.

Although the regime of the RBC could also be dependent on two other parameters, the Prandtl number defined as:

$$Pr = \frac{\nu}{\kappa} \tag{2}$$

and the shape of the cell [2], most of the turbulent regimes are reported for $Ra > 10^5$ [2].

III. Experiment Methodology

The enclosure used for this experiment is shown in Fig. 2. The enclosure is made by 6.3 mm thick acrylic sheet with the dimension of 50 × 50 × 50 mm^3 for having optical access to apply PIV measurement technique on the flow. The hot and cold flow from two controlling water baths pass through two heat exchangers consisting of 3 mm copper sheets are used as the heat source and sink. The temperature of the cold flow is set to 5 °C and the hot flow is set to 35 °C. The working fluid is water with the initial temperature of the ambient and equal to 21.3 °C. The working fluid used for this experiment is distilled degassed water. The properties of the working fluid with the temperature condition of the two hot and cold surfaces are shown in Table. 1. In this table, T_M is the ambient temperature and the initial temperature of the fluid.

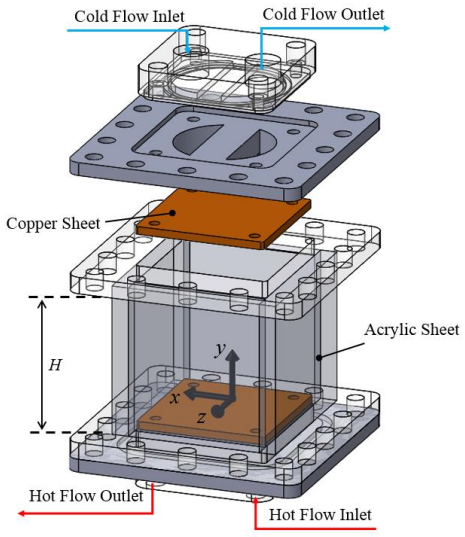

Figure 1. RBC enclosure used for the experiment

To make sure that the heat source and sink used in this experiment generate a continuous distribution of the temperature, an IR camera (FLIR A35, FLIR Systems Inc.) is used to visualize the temperature distribution on the copper surface. Fig. 3 shows the non-dimensional temperature distribution on the copper surface. The standard deviation of the temperature distribution on the surface is found to be around 1.7 %. Based on Fig. 3, there are four regions showing lower temperature in comparison to the average temperature distribution which are located where the 4 mm bolts fix the copper sheet to the base of the heat-exchanger. The temperature distribution of this region is found to be 7 % lower than the other region of the surface.

Sidewalls of the enclosure are assumed to be adiabatic in RBC studies. The walls of the enclosure used in this experiment is made of acrylic sheet which has low thermal conductivity (0.2 W/mK). Furthermore, the temperature of the ambient is monitored during the experiment to make sure that the temperature difference between the sidewalls and the ambient is kept constant. To do this, a thermocouple is used located close to the surface of one of the sidewalls. At the start of the experiment, the temperature of the ambient is equal to 21.3 °C, the standard deviation of the temperature fluctuations during the experiment is ~ 2.3%.

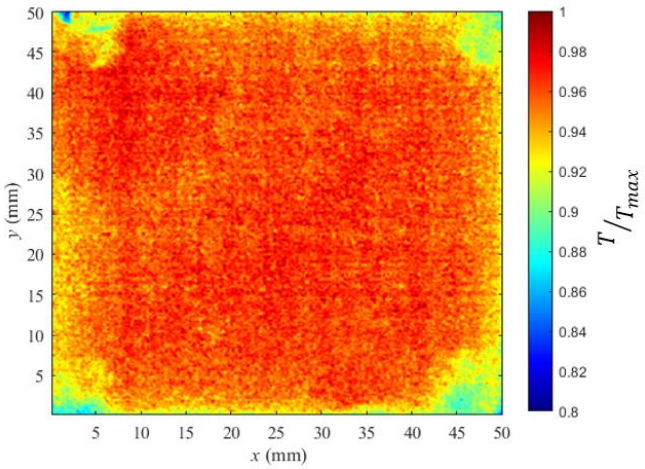

Figure 2. Normalized temperature distribution on the copper plate.

Fig. 4 shows a schematic of the optical measurement system used to apply PIV. A high-speed CMOS camera (Flare 12M125, IO Industries Inc.) with a maximum frame rate of 220 fps is used to capture the flow field. An external hard drive is synced with the camera for high-speed data transfer, making the long duration of continuous high-speed imaging possible. A standard SLR camera lens (50mm Nikkor, Nikon Inc) was connected to the camera to image the region of interest.

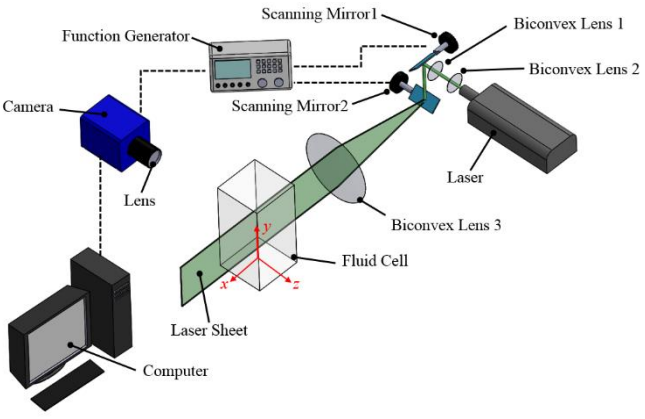

Figure 3. Experimental setup schematic.

TABLE.I Working fluid and temperature and geometrical properties of the experiment

Parameter	T_H (°C)	T_C (°C)	T_M (°C)	α (°C^{-1})	κ (m^2.s^{-1})	ν (m^2.s^{-1})	H (m)	Pr	Ra
Value	35	5	21.3	2.14×10^{-4}	1.4×10^{-7}	9.98×10^{-7}	0.05	6.98	5.5×10^{7}

To illuminate the seeded flow field, a continuous Argon-ion laser turned to operate at 488 nm wavelength was used. As is shown in Fig. 4, two biconvex lenses are also set to control the thickness of the laser beam. Two scanning mirrors were used to generate the laser sheet (scanning mirror 2) and control the location of it in the *z*-direction to be at $z = 0$. Biconvex lens 3 is used to make the laser sheet parallel to the *x*-*y* plane. Both scanning mirrors and the camera are connected to a function generator to sync the frequency of the camera with the scanning mirror 2, and to control the scanning mirror 1. This approach is further described in [19].

IV. RESULTS AND DISCUSSION

A. Final State

A false colour map of the magnitude of velocity is shown in Fig. 5 *x*-*y* plane at the half depth, $z = 0$ mm of the enclosure for $t_1 = 2450$ s to $t_2 = 2800$ s. Streamlines are overlaid to highlight the counterclockwise mean wind or LSC. With the hot source at the bottom of the images and the cold source at the top, the direction of rotation can be identified by the two small vortices at the top-right (labelled as A) and bottom-left (labelled as B) of the flow. A stagnation region skewed from the centre to the top-left (labelled as C) shows that the mean wind is occurring in a plane slightly angled from the *x*-*y* plane rotated around the *y*-axis. In confined enclosures, the stagnation area is typically found exactly at the centre showing rotation of the mean wind around the *z*-axis [15].

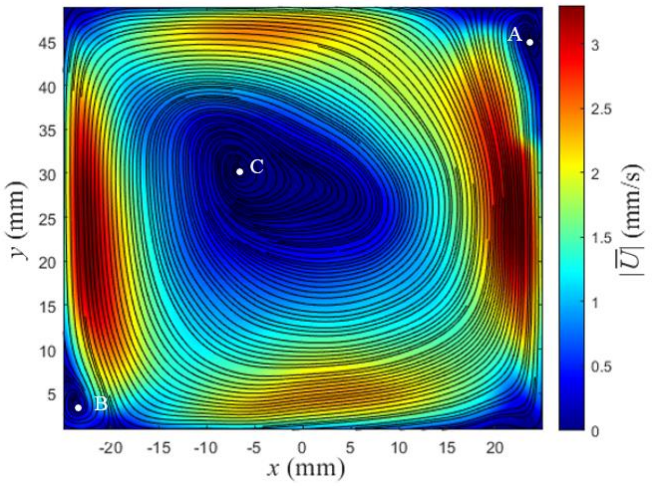

Figure 4. Mean velocity of the flow field.

Variation of the mean velocity profile, $|\overline{U}|$ is shown in Fig. 6 (a) at the two centre lines of $x = 0$ mm and $y = 25$ mm. From this plot and Fig. 5, it can be observed that the maximum velocity is occurring at the side walls close to the walls which reaches up to 3.4 mm/s. There are also two high-velocity horizontal regions at the top and bottom of the enclosure reaching the maximum velocity of 2.4 mm/s at the vertical centreline. At the horizontal centreline, minimum velocity reaches 0.3 mm/s and at the vertical centreline that is equal to 0.05 m/s. The location of the stagnation point which is the centre of the LSC is at $x = -6$ mm and $y = 30$ mm.

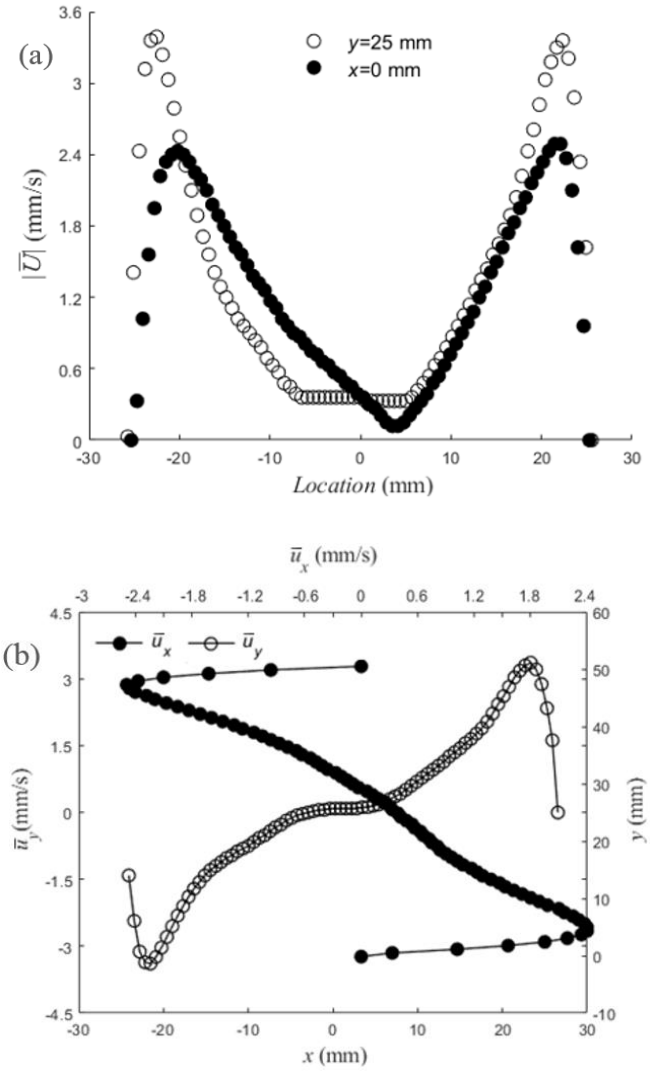

Figure 5. (a) Mean velocity profile at the two centre lines. (b) Mean vertical velocity profile at the horizontal centreline $y = 0$ and mean horizontal velocity profile at the vertical centreline $x = 0$.

The variation of the mean vertical velocity profile $\bar{u}_y$, at the horizontal centre line and the mean horizontal velocity $\bar{u}_x$, at the vertical centre line is shown in Fig. 6 (b). It can be observed that both of the mean velocity profiles are symmetric. The

maximum value of the mean vertical velocity profile, $\bar{u}_y$, is equal to 3.6 mm/s and it is equal to 2.4 mm/s for the mean horizontal velocity, $\bar{u}_x$. The measured velocity profile of both Fig.6 (a) and (b) have an agreement with both the shape of the velocity profile at the sidewalls and at the top and bottom reported by the Valencia et al. [17] for $Ra = 7 \times 10^7$ which is close to the conditions of the conducted experiment. The value of the maximum velocities also have an agreement whit the experimental results of them.

B. Initial flow development

The mean velocity field distribution at *x-y* plane at the half depth, $z = 0$ of the enclosure for $t_1 = 200$ s to $t_2 = 340$ s is shown in Fig. 7. As can be observed, the mean flow structure is generally symmetric with respect to the vertical centreline, $x = 0$. Two large scale counter-rotating structure are formed at the half-bottom of the RBC cell. As a result of these two large scale vortices, a stagnation region is formed at the centre-bottom of the RBC cell. In the half-top of the RBC cell, as can be observed tracking the mean velocity vectors, the mean flow is moving to the top surface which is the cooling surface. Due to this, two small vortices are formed at the corners of this region.

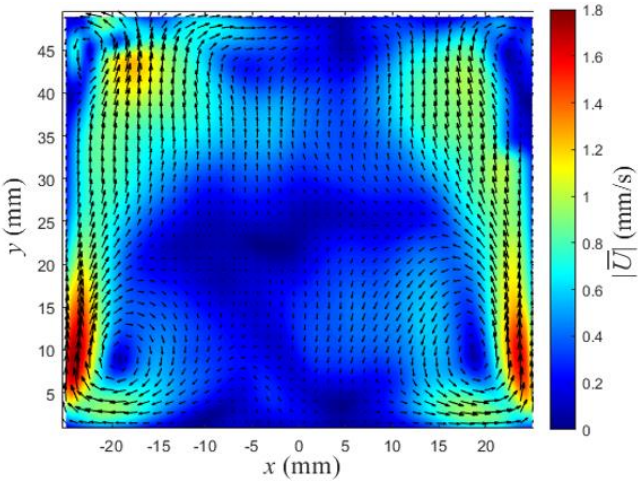

Figure 6. Mean velocity of the flow field.

The mean kinetic energy, $\overline{KE} = \frac{1}{2}|\bar{U}||\bar{U}|$ of the entire flow field is plotted as it varies with time Fig. 8. The mean kinetic energy convergence zone is considered from $t = 200$ s which is shown in Fig. 8 with the dashed line. The mean velocity field distribution shown in Fig. 7 is defined based on this criterion. At the start, flow is stationary and $\overline{KE} = 0$. After the start of heating and cooling of the bottom and top surfaces, the thermal plumes start rising from the bottom surface and falling from the top surface [5].

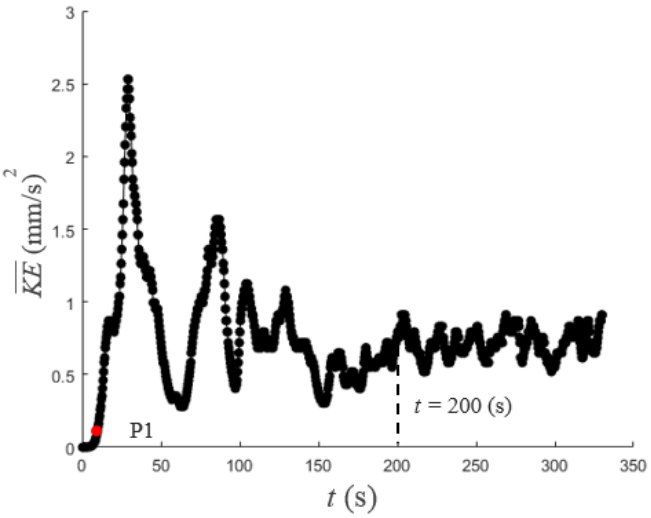

Figure 7. Averaged kinetic energy fluctuations during the onset of convection.

From Fig. 8 a mean flow with a mean flow structure can be expected. The time scale of the flow from the onset to the first mode of mean flow is on the order of a hundred seconds. However, the change in the mode of the flow has been reported in the time scale of thousands of seconds [5] to ten thousand seconds [18]. These different orders of the time scale show the existence of the LSC in different time scales even at the onset of the convection which is shown in this study.

The starting state of the formation of the thermal plumes is shown as P1 in Fig. 8. The instantaneous velocity distribution for this state is shown in Fig. 9. The flow structure of this state can be divided into the top and bottom region result in the thermal plumes rising and falling from the hot and cold surface respectively. At each region, two primary plumes can be observed which each of them leads to the formation of a pair of counter-rotating flow structure. From the colour map, it can be inferred that the hot plumes carrying more kinetic energy in comparison with the cold plumes. This also can be observed in the mean flow structure in Fig. 7 which shows the dominancy of the hot plumes.

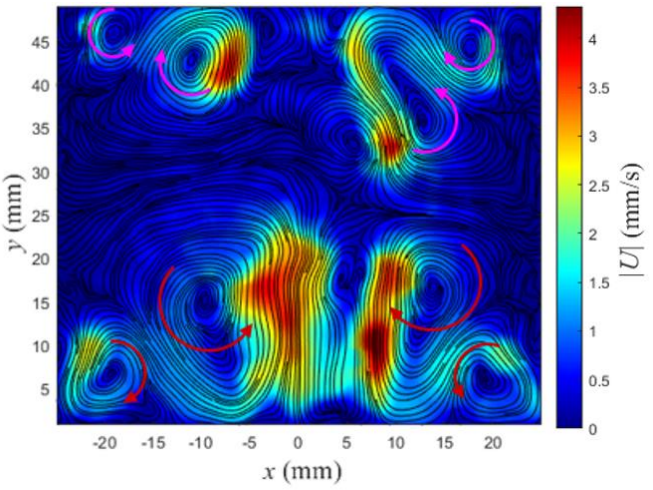

Figure 8. The instantaneous velocity of the flow field at the onset of convection.

V. CONCLUSION

An experiment conducted to investigate the flow topology of the turbulent RBC (Rayleigh-Benard Convection) in a cubical enclosure with unit aspect ratio. The mean flow structure of the flow known as the mean wind compared with the mean flow structure at the onset of the convection showing the dominancy of the hot plumes in this experiment flow condition which led to the finding of a symmetrical flow structure during the start of the RBC.

ACKNOWLEDGMENTS

The authors acknowledge financial support from Future Energy Systems (FES) and the Natural Sciences and Engineering Research Council (NSERC) of Canada.

REFERENCES

[1] B. Adrian, CONVECTION HEAT TRANSFER. John Wiley and Sons, Inc. 2013.

[2] L. A. Couston, D. Lecoanet, B. Favier, and M. Le Bars, "Shape and size of large-scale vortices: A universal fluid pattern in geophysical fluid dynamics," *Phys. Rev. Res.*, vol. 2, no. 2, p. 23143, 2019.

[3] D. Lohse and K. Q. Xia, "Small-scale properties of turbulent Rayleigh-Benard convection," *Annu. Rev. Fluid Mech.*, vol. 42, pp. 335–364, 2010.

[4] I. V. Miroshnichenko and M. A. Sheremet, "Turbulent natural convection heat transfer in rectangular enclosures using experimental and numerical approaches: A review," *Renew. Sustain. Energy Rev.*, vol. 82, no. December 2016, pp. 40–59, 2018.

[5] K. Xia, "From laminar plumes to organized flows: the onset of large-scale circulation in turbulent thermal convection," *J. Fluid Mech.*, vol. 503, pp. 47–56, 2004.

[6] J. Pallares, M. P. Arroyo, F. X. Grau, and F. Giralt, Experimental laminar Rayleigh-Benard convection in a cubical cavity at moderate Rayleigh and Prandtl numbers," *Exp. Fluids*, vol. 31, no. August 1998, pp. 208–218, 2001.

[7] S. Zhou, C. Sun, and K. Xia, "Measured oscillations of the velocity and temperature fields in turbulent Rayleigh-Benard convection in a rectangular cell," *Phys. Rev. E*, pp. 28–30, 2007.

[8] R. Yang, K. L. Chong, Q. Wang, R. Verzicco, O. Shishkina, and D. Lohse, "Periodically modulated thermal convection," Phys. Rev. Lett., no. 1, pp. 1–5, 2020.

[9] S. Weiss and G. Ahlers, "Effect of tilting on turbulent convection : cylindrical samples with aspect ratio Γ = 0 . 50," *J. Fluid Mech.*, pp. 314–334, 2013.

[10] Q. Wang, R. Verzicco, D. Lohse, and O. Shishkina, "Multiple states in turbulent large-aspect ratio thermal convection: What determines the number of convection rolls?," *Phys. Rev. Lett.*, pp. 1–6, 2020.

[11] L. Zwirner and O. Shishkina, "Confined inclined thermal convection in low-Prandtl-number fluids," *J. Fluid Mech.*, vol. 1, pp. 984–1008, 2018.

[12] E. P. Van Der Poel, R. J. A. M. Stevens, and D. Lohse, "Connecting flow structures and heat flux in turbulent Rayleigh-Benard convection," *Phys. Rev. E*, vol. 045303, pp. 1–4, 2011.

[13] A. You, M. A. Y. Be, and I. In, "Flow states in two-dimensional Rayleigh- Benard convection as a function of aspect- ratio and Rayleigh number," *Phys. Fluids*, vol. 085104, no. April 2012, 2016.

[14] C. Kästner, C. Resagk, J. Westphalen, M. Junghähnel, and C. Cierpka, "Assessment of horizontal velocity fields in square thermal convection cells with large aspect ratio," *Exp. Fluids*, vol. 59, no. 11, pp. 1–13, 2018.

[15] K. Xia, C. Sun, and S. Zhou, "Particle image velocimetry measurement of the velocity field in turbulent thermal convection," *Phys. Rev. E*, no. August, pp. 1–18, 2003.

[16] V. Valori, G. Elsinga, M. Rohde, M. Tummers, J. Westerweel, and T. Van Der Hagen, "Experimental velocity study of non-Boussinesq Rayleigh-Benard convection," *Phys. Rev. E*, vol. 053113, pp. 1–12, 2017.

[17] L. Valencia, J. Pallares, I. Cuesta, and F. X. Grau, "Turbulent Rayleigh – Benard convection of water in cubical cavities : A numerical and experimental study," *Int. J. Heat Mass Transf.* vol. 50, pp. 3203–3215, 2007.

[18] H. Xi, Q. Zhou, and K. Xia, "Azimuthal motion of the mean wind in turbulent thermal convection," *Phys. Rev. E*, no. February, pp. 1–13, 2006.

[19] M. A. Kazemi, D. S. Nobes, and J. A. W. Elliott, "Experimental and numerical study of the evaporation of water at low pressures," *Langmuir*, vol. 33, no. 18, pp. 4578–4591, 2017.